Propulsion generated by diffusion-driven flow

Michael R. Allshouse[1], Michael F. Barad[2] and Thomas Peacock[1]★

Buoyancy-driven flow, which is flow driven by spatial variations in fluid density[1], lies at the heart of a variety of physical processes, including mineral transport in rocks[2], the melting of icebergs[3] and the migration of tectonic plates[4]. Here we show that buoyancy-driven flows can also generate propulsion. Specifically, we find that when a neutrally buoyant wedge-shaped object floats in a density-stratified fluid, the diffusion-driven flow at its sloping boundaries generated by molecular diffusion produces a macroscopic sideways thrust. Computer simulations reveal that thrust results from diffusion-driven flow creating a region of low pressure at the front, relative to the rear of an object. This discovery has implications for transport processes in regions of varying fluid density, such as marine snow aggregation at ocean pycnoclines[5], and wherever there is a temperature difference between immersed objects and the surrounding fluid, such as particles in volcanic clouds[6].

A fluid system with spatially varying density, resulting from temperature and/or salinity variations, for example, is stably-stratified when increasing density is parallel to the direction of gravity. When an object is released in a quiescent, stably-stratified fluid, it is expected to settle or rise to the neutral buoyancy level at which the density of the object matches that of the surrounding fluid, and remain stationary thereafter. We carried out a control experiment in which a 19.05-mm-diameter sphere of density $\rho = 1{,}115\,\mathrm{kg\,m^{-3}}$ was released in a tank of height $H = 0.40\,\mathrm{m}$, width $W = 0.20\,\mathrm{m}$ and length $L = 0.40\,\mathrm{m}$, filled with salt-stratified water with density gradient $\mathrm{d}\rho/\mathrm{d}z = -511 \pm 3\,\mathrm{kg\,m^{-4}}$. As expected, the sphere settled to its neutral buoyancy height, where it remained stationary for 24 hours. A similar experiment was then carried out using a triangular wedge (Fig. 1) of length $l = 99.9 \pm 0.1\,\mathrm{mm}$, base $h = 17.6 \pm 0.10\,\mathrm{mm}$ (corresponding to slope angle $\alpha = 5.0 \pm 0.1°$) and width $w = 25.1 \pm 0.10\,\mathrm{mm}$. In striking contrast to the stationary sphere, the wedge moved at a constant speed $u = 10.2 \pm 0.1 \times 10^{-3}\,\mathrm{m\,h^{-1}}$ ($2.83 \pm 0.03 \times 10^{-6}\,\mathrm{m\,s^{-1}}$) in the direction of its tip, without any obvious cause (Fig. 1 and its top inset; also see Supplementary Movie S1).

To investigate the cause of this spontaneous propulsion, we visualized the velocity fields in the horizontal and vertical mid-planes of the moving wedge using particle image velocimetry (PIV; Fig. 2). Here, z is the vertical coordinate antiparallel to gravity and x and y are the coordinates in the horizontal plane, parallel and perpendicular to the long axis of the wedge, respectively. These experiments reveal that fluid is drawn in towards the wedge tip in the horizontal plane to supply up-slope flow in a thin boundary layer above the sloping surface. Furthermore, fluid immediately behind the wedge moves with the same speed as the wedge; this phenomenon, known as blocking, occurs for obstacles in stratified flow when buoyancy forces dominate inertia and viscous forces[1]. As a whole, these experiments reveal a localized flow field that extends $\sim$50 mm in front and behind, $\sim$30 mm above and below and $\sim$80 mm to either side of the moving wedge.

The up-slope flow in Fig. 2 reveals the cause of propulsion to be diffusion-driven flow[2,7]. This is a buoyancy-driven flow that occurs when a stably-stratified fluid encounters a sloping boundary, for the following reason. Molecular diffusion requires that surfaces of constant density (isopycnals) approach a sloping boundary at an appropriate angle to ensure continuity of diffusive flux across the boundary. For the triangular wedge that is impermeable to salt, isopycnals must be locally perpendicular to the slope to satisfy the no-flux boundary condition $\partial\rho/\partial\eta = 0$, where η is the wall-normal coordinate (Fig. 1, bottom inset). Fluid adjacent to the sloping boundary therefore differs in density to fluid at the same level away from the boundary, and experiences a buoyancy force that drives flow up- or down-slope for underlying and overlying walls, respectively, the kinetic energy of motion being drawn from the internal energy of the fluid through diffusion.

For constant slope, and assuming along-slope flow that is a function only of the wall-normal coordinate (that is, unidirectional flow), the velocity profile for steady diffusion-driven flow is[2,7] $\tilde{u}(\eta) = u_0 e^{-\gamma\eta}\sin(\gamma\eta)$, where $u_0 = 2\kappa\gamma\cot\alpha$ is the characteristic tangential flow velocity, $\gamma^{-1} = (N^2\sin^2\alpha/4\nu\kappa)^{-1/4}$ is the boundary-layer thickness, $N = \sqrt{-g/\rho_0(\mathrm{d}\rho/\mathrm{d}z)}$ is the buoyancy frequency, ρ_0 is the characteristic fluid density, κ is the molecular diffusivity and ν is the kinematic viscosity. The characteristic scales of u_0 and γ^{-1} for a salt stratification ($\kappa \sim 10^{-9}\,\mathrm{m^2\,s^{-1}}$, $\nu \sim 10^{-6}\,\mathrm{m^2\,s^{-1}}$) are $1 \times 10^{-5}\,\mathrm{m\,s^{-1}}$ and 0.1 mm, respectively, consistent with the PIV visualization (Fig. 2); for a thermal stratification ($\kappa \sim 10^{-7}\,\mathrm{m^2\,s^{-1}}$, $\nu \sim 10^{-6}\,\mathrm{m^2\,s^{-1}}$), these scales increase to $1 \times 10^{-3}\,\mathrm{m\,s^{-1}}$ and 0.3 mm, respectively.

Motivated by the observation of a localized flow field around the wedge, our experiments found that for $L/l > 2$, $W/w > 6$ and $H/h > 5$ the propulsion speed u is independent of the size of the experimental tank, and the wedge behaves as if unconfined (see Supplementary Information). In this limit, there are eight variables on which u can depend ($\rho, \mathrm{d}\rho/\mathrm{d}z, g, \nu, \kappa, \alpha, l, w$), and through the combination of experiment and dimensional analysis we seek to establish what sets u. Buckingham's pi-theorem[8] requires six independent dimensionless parameters that characterize the system. Although there is freedom in selecting these, five natural choices are: the shape parameters α and w/l, the ratios of viscous and buoyancy forces to inertia forces, $\mathrm{Re} = u_0 l/\nu$ and $\mathrm{Fr} = u_0/Nl$, respectively referred to as the Reynolds and Froude numbers, and the ratio of molecular and viscous diffusivity, $\mathrm{Sc} = \nu/\kappa$, referred to as the Schmidt number. Choosing the dimensionless speed u/u_0 as the final dimensionless parameter, we investigate the functional relation $u/u_0 = f(\alpha, w/l, \mathrm{Re}, \mathrm{Fr}, \mathrm{Sc})$.

In the first set of experiments, for the wedge shown in Fig. 1, it was found that $u \propto (-\mathrm{d}\rho/\mathrm{d}z)^{0.25 \pm 0.02}$ for stratifications using KCl ($\mathrm{Sc} = 527$), NaCl ($\mathrm{Sc} = 810$) and $MgCl_2$ ($\mathrm{Sc} = 1{,}592$); the results are shown in Fig. 3a. Thus, u/u_0 is a constant for each stratifying agent, because u_0 scales similarly with the stratification.

[1]Department of Mechanical Engineering, Massachusetts Institute of Technology, 77 Massachusetts Avenue, Cambridge, Massachusetts 02139, USA, [2]Environmental Fluid Mechanics Laboratory, Stanford University, Yang & Yamasaki Environment & Energy Building, 473 Via Ortega, Office M15, Stanford, California 94305, USA. *e-mail: tomp@mit.edu.
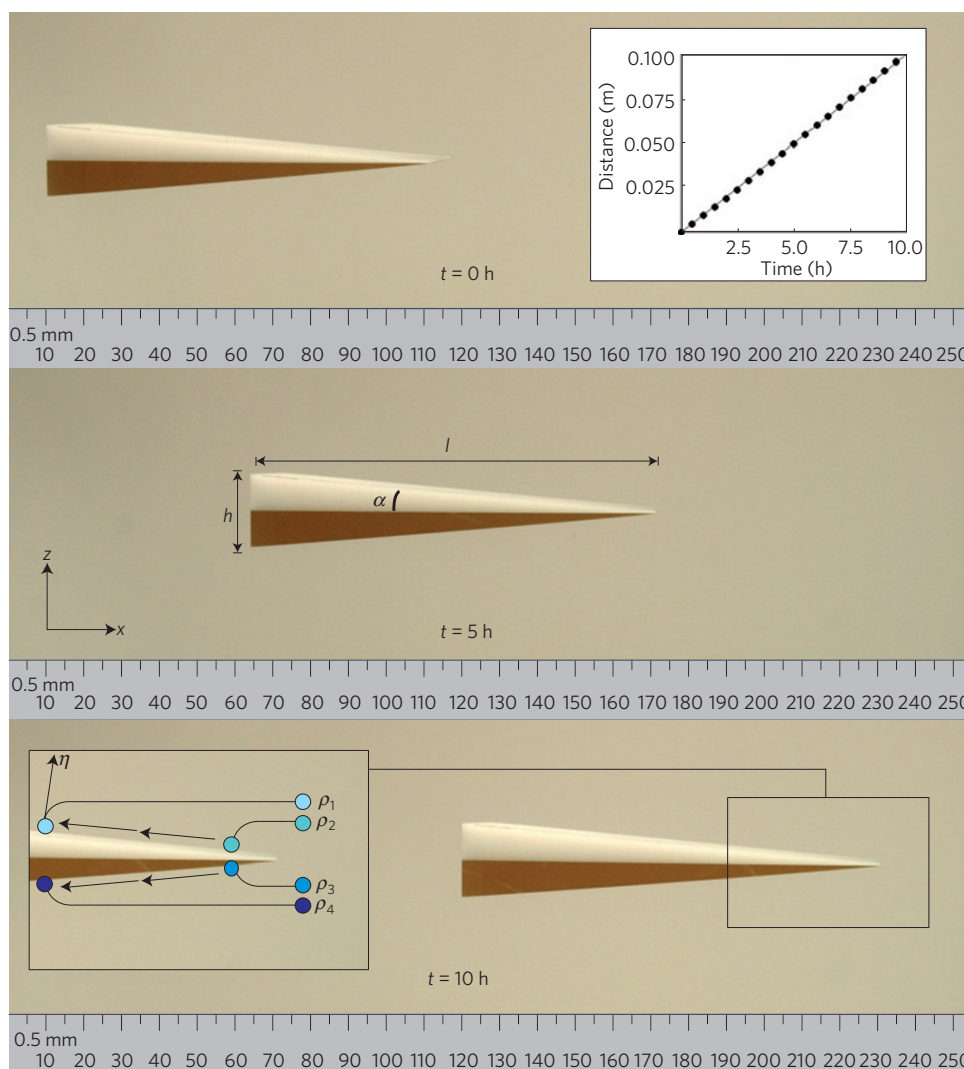
Figure 1 | Spontaneous propulsion of a triangular wedge in a density-stratified fluid. A three-image sequence for a triangular wedge ($l = 99.9$ mm, $h = 17.6$ mm ($\alpha = 5.0°$), $w = 25.1$ mm) floating in salt-stratified water with density gradient $d\rho/dz = -511$ kg m^{-4}. The wedge is spontaneously propelled with speed 10.2×10^{-3} m h^{-1}. Top inset: The data points (filled circles) show the measured position of the wedge tip as a function of time. Bottom inset: The sloping surfaces of the wedge alter the local fluid density because diffusion requires that lines of constant density arrive perpendicular to the surface. A fluid element of density ρ_1 (ρ_4) next to the slope is therefore at the same height as fluid of density ρ_2 (ρ_3) away from the slope, and experiences a buoyancy force that drives flow up (down)-slope, as indicated by the arrows.

These results reveal that $u/u_0 = f(\alpha, w/l, \mathrm{Sc})$ is independent of Re and Fr. Furthermore, using the wedge shown in Fig. 1, the second set of experiments found that within experimental uncertainty u/u_0 is independent of Sc for $527 < \mathrm{Sc} < 3{,}143$ (Fig. 3b), and thus $u/u_0 = f(\alpha, w/l)$ depends only on the wedge shape for the range of Schmidt numbers investigated. For our third set of experiments, several different-shaped wedges were used to investigate the effect of varying the aspect ratio w/l for a constant slope angle ($\alpha = 5°$) and constant NaCl stratification ($d\rho/dz = -460$ kg m^{-4}). It was found that the propulsion speed u increases noticeably with increasing w/l (Fig. 3c) and, consistent with the prediction of dimensional analysis, is independent of wedge size, as demonstrated by the results obtained for wedges of the same aspect ratio but different size. The final set of experiments determined that for a constant aspect ratio ($w/l = 0.25$) and NaCl stratification ($d\rho/dz = -460$ kg m^{-4}), the propulsion speed u drops off rapidly with increasing α (Fig. 3d), because an increasing slope angle both decreases the strength of diffusion-driven flow and increases drag by virtue of increasing the size of the wedge. Significantly, for $\alpha < 5°$ there is a diminution in the rate at which

u increases with decreasing α, coinciding with the breakdown of diffusion-driven flow[9].

To determine the origin of thrust, we carried out a three-dimensional (3D) numerical simulation of diffusion-driven flow around a fixed wedge. The simulation used essentially the same configuration as the experiments in Fig. 1, with the one exception being $\mathrm{Sc} = 1$ rather than $\mathrm{Sc} \approx 1{,}000$, as the former is more tractable numerically. In contrast to the boundary-layer solution, $u_0(\eta)$, which applies only to a semi-infinite domain and produces no thrust, there is an intricate flow field with characteristic flow speeds of 1×10^{-3} m s^{-1} surrounding the wedge (Fig. 4a). This flow field is similar to $u_0(\eta)$ within the boundary-layer scale ($\gamma^{-1} \approx 2$ mm) over most of the top and bottom sloping surfaces, with a slight ($\sim$25%) reduction in peak velocity. The flow field diverges noticeably from the analytical form within two millimetres of the sides, front and rear of the wedge, as well as outside the boundary layer, where fore–aft-asymmetric flow structures exist to balance the rearward volume flux along the sloping surfaces[10,11]; the same qualitative features are present in our PIV data set (Fig. 2a). Asymmetric density-field perturbations of the order of $\Delta\rho \approx 0.1$ kg m^{-3} are
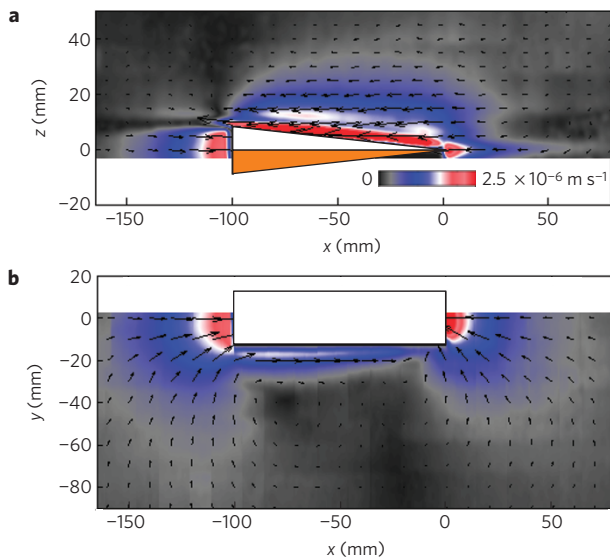
Figure 2 | PIV visualizations of the flow field around a moving wedge.
a,b, Velocity fields in the vertical (**a**) and horizontal (**b**) mid-plane of the wedge moving with speed 2.3×10^{-6} m s^{-1} (8.3×10^{-3} m h^{-1}) as a result of a background stratification of $d\rho/dz = -350$ kg m^{-4}. The colour map is saturated at 2.5×10^{-6} m s^{-1} to facilitate visualization of the whole flow field; maximum speeds of the order of 1×10^{-5} m s^{-1} were detected immediately above the sloping surface. The velocities are presented in the laboratory frame of reference, in which the wedge is moving, and the origin of the coordinate system lies at the centre of the wedge tip at this instant in time.

induced by the flow field[10,11] (Fig. 4b), creating a hydrostatic pressure drop of $\Delta p \approx 10$ mPa on the sloping surfaces (Fig. 4c). The thrust on the fixed wedge because of this pressure drop exceeds everywhere the viscous stresses associated with the boundary-layer flow, and there is a net forward force $F \approx 0.4\,\mu$N that is calculated from the numerical data using a control volume containing the wedge. A related mechanism has recently been proposed for the propulsion of colloidal particles by virtue of a surface chemical reaction creating a lateral osmotic-pressure imbalance[12].

To estimate the propulsion speed resulting from the thrust, we carried out a numerical simulation that calculated the drag on a slowly moving wedge, finding that a propulsion speed $u \approx 4.5 \times 10^{-4}$ m s^{-1} produces a drag of $0.4\,\mu$N for the wedge in Fig. 1. This propulsion speed gives $u/u_0 \sim 0.02$, which is consistent with the experimental result obtained for larger values of Sc than the numerical simulation. We note that this mechanism rationalizes why the propulsion speed is only a function of aspect ratio (and not size), because both thrust and viscous drag scale proportionally with the dimensions of the wedge. Furthermore, we recognize that propulsion occurs because of the asymmetric shape of the wedge; a symmetric object, such as a sphere, remains stationary because there is no unbalanced horizontal force produced by diffusion-driven flow.

Our discovery that a propulsive force can arise on any floating object that influences the surrounding fluid density greatly broadens the scope of buoyancy-driven flow, and such a fundamental discovery inevitably opens many avenues for future research. For example, we investigated density stratifications resulting from salinity variations, for which Sc > 500. Extrapolating these results, one might anticipate significantly faster propulsion speeds for an insulating wedge in a thermal stratification (Sc $\approx$ 7). Another related scenario that is commonplace in nature is a floating object that is hotter or colder than the surrounding fluid, in which case the resulting surface flows, analogous to valley[13] and glacier winds[14], are
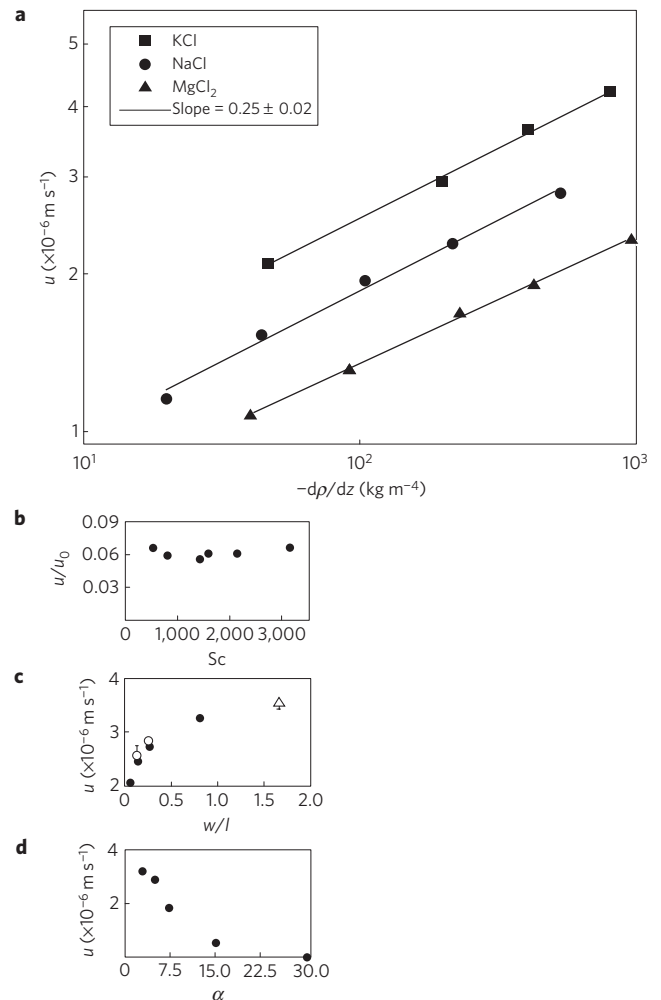

Figure 3 | Experimental results for u as a function of the governing parameters. a, $u \propto (-d\rho/dz)^{0.25\pm0.02}$ for stratifications using KCl (Sc = 527), NaCl (Sc = 810) and MgCl$_2$ (Sc = 1,592) for the wedge in Fig. 1. **b**, The dimensionless speed u/u_0 varies little with Sc for the wedge in Fig. 1. **c**, For a fixed slope angle ($\alpha = 5°$) and constant NaCl stratification ($d\rho/dz = -460$ kg m^{-4}), u increases with increasing w/l for $w = 12.5$ mm (filled circles), $w = 25.1$ mm (open circles) and $w = 50.0$ mm (open triangles). Note that u is the same for experiments with different w but the same w/l. **d**, For a constant aspect ratio ($w/l = 0.25$) and NaCl stratification ($d\rho/dz = -460$ kg m^{-4}), there is a sharp drop in u as a function of increasing α. There is also a noticeable change in the trend around $\alpha = 5°$, coinciding with the known breakdown of diffusion-driven flow[9]. The error bars in all of the panels represent standard deviations, and in most cases they are smaller than the symbol size.

much stronger than diffusion-driven flow, also raising the prospect of significantly faster propulsion speeds. Indeed, if sufficiently large thrusts can be produced by surface heating and cooling, this could enable the design of silent underwater vehicles without any moving mechanical components. In another set of (preliminary) experiments, we found that interactions occur between a pair of wedges (see Supplementary Information), suggesting a new mechanism for collective behaviour of floating objects. Finally, an important avenue to explore is the energy balance of these processes. It is particularly interesting that in our experiments the kinetic energy of macroscale motion is actually drawn from the internal energy of the fluid via microscale molecular diffusion. This influences internal and gravitational potential energies of the system, and could connect with present debate regarding ocean energetics[15].
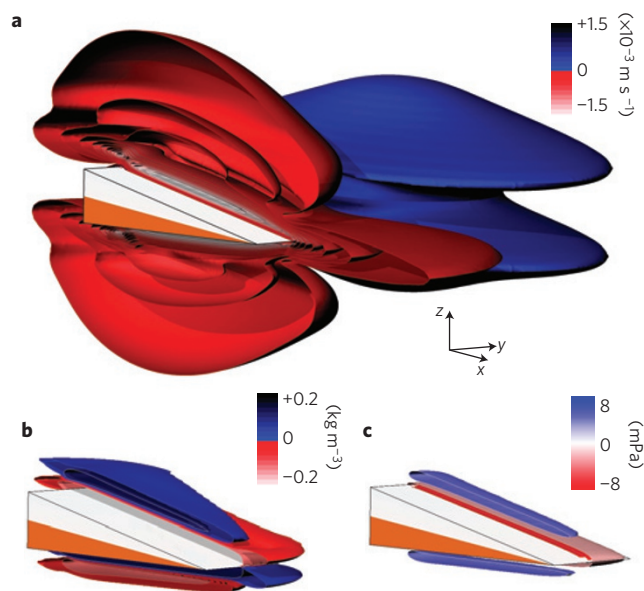
Figure 4 | Numerical simulation of diffusion-driven flow induced by a fixed wedge. Except for the Schmidt number (Sc = 1) and a slight change in the stratification ($d\rho/dz = -546$ kg m^{-4}), all parameters are the same as in Fig. 1. **a**, Iso-surfaces of the x component of horizontal velocity reveal intricate flows of characteristic speed 1×10^{-3} m s^{-1} that surround the wedge. **b**, Iso-surfaces of density perturbations of the order of $\Delta\rho \approx 0.1$ kg m^{-3} relative to the far-field stratification. **c**, Iso-surfaces of pressure perturbations of the order of $\Delta p \approx 10$ mPa relative to the far-field pressure. In contrast to the unaffected pressure field behind the wedge, regions of low hydrostatic pressure arise on the sloping surfaces because of the perturbations to the surrounding density field. This pressure drop everywhere exceeds the viscous stress owing to diffusion-driven flow, resulting in a net thrust of 0.4 µN on the fixed wedge.

Methods

General. The upper and lower halves of each wedge were machined from high-density polyethylene ($\rho = 955$ kg m^{-3}) and Ultem 1,000 polyetherimide ($\rho = 1,280$ kg m^{-3}), respectively; this ensured that a wedge's centre of gravity lay below its centre of buoyancy, producing a stabilizing torque that maintained a horizontal orientation. A stratification was established using the double-bucket method and measured by a calibrated conductivity and temperature probe. At the start of an experiment, a cage of six vertical, 35-cm-long stainless-steel rods was lowered slowly ($\sim 1 \times 10^{-3}$ m s^{-1}) into the stratification using a computer-controlled traverse. The wedge initially settled within the confine of the rods. The system was left to stand for one hour before the cage was withdrawn slowly, leaving the wedge floating in the quiescent stratification. The top of the experimental tank was sealed to eliminate atmospheric disturbances. Horizontal motion of the wedge was photographed from above, the length of the wedge providing a calibration length scale in each image.

Schmidt number. Experiments were run for different Schmidt numbers (Sc = ν/κ) by using different salts (KCl, NaCl, MgCl$_2$) dissolved in water, and by using NaCl dissolved in water/glycerol mixtures. The kinematic viscosity, ν, was measured using an Ostwald viscometer. The molecular diffusivity, κ, was measured by establishing a density stratification and introducing a triangular ledge that spanned the entire width of the tank, so as to induce a nominally 2D flow. The ledge had upper and lower slope angles of $\alpha = 10.0 \pm 0.1°$ with respect to the horizontal plane. The volume flux drawn towards the tip of the ledge in the vertical mid-plane, Q, was measured using PIV, and κ was calculated using the relation $Q = 2\kappa \cot\alpha$.

Visualizations. A LaVision PIV system was used to obtain flow visualizations in the vertical and horizontal mid-plane of the wedge. The stratification was seeded with 10-µm glass spheres, with a range of densities, the motion of which was tracked to obtain velocity field data. Given the slow flow speeds, to ensure that data were not contaminated by particle settling, the stratification was left to stand for four days after filling, allowing sufficient time for particles to reach their neutral buoyancy heights.

Numerical simulations. 3D numerical simulations of stratified flow past a fixed wedge were computed using an adaptive, block-structured, two-way nested, second-order accurate finite-volume method[16]. This method is designed for the study of flows that are multiscale, incompressible, of variable density and within arbitrarily complex domains. The 3D simulations were run on a Cray XT4 supercomputer. The 3D computational fluid dynamics flow domain was a $0.3 \times 0.3 \times 0.3$ m^3, with the wedge tip centre located at $x = 0.17$ m, $y = 0.15$ m, $z = 0.15$ m from the lower corner of the cube. The mesh was locally refined using block-structured refinement, the finest scale of the mesh along the wedge being 5.8×10^{-4} m, yielding an effective resolution of 134 million cells. Insulating, no-slip boundary conditions were imposed on the wedge. To determine that the simulations had achieved a steady state, time series of both the force on the wedge and the total kinetic energy of the flow around the wedge were calculated. The system was considered to be in a steady state when both of these quantities varied by less than 1% over a physical timescale of 1,000 s.

A 3D COMSOL simulation was used to calculate the drag on a slowly moving wedge in homogeneous water. The wedge was fixed in the centre of the domain. The front of the domain had constant-velocity inlet conditions and the rear of the domain had outlet boundary conditions. All of the sidewalls had stress-free boundary conditions to remove boundary layer effects. The size of the domain and the mesh resolution were increased until each had a less than 1% impact on the drag. The calculation of the drag was provided by the COMSOL software, by means of boundary integration on the surfaces of the wedge, which was independently checked using our own control volume approach.

References

1. Turner, J. S. *Buoyancy Effects in Fluids* (Cambridge Univ. Press, 1973).
2. Phillips, O. M. On flows induced by diffusion in a stably stratified fluid. *Deep-Sea Res.* **17,** 435–443 (1970).
3. Huppert, H. E. & Turner, J. S. On melting icebergs. *Nature* **271,** 46–48 (1978).
4. Gurnis, M. Large-scale mantle convection and the aggregation and dispersal of supercontinents. *Nature* **332,** 695–699 (1988).
5. MacIntyre, S., Alldredge, A. L. & Gotschalk, C. C. Accumulation of marine snow at density discontinuities in the water column. *Limnol. Oceanogr.* **40,** 449–468 (1995).
6. Hoyal, D. C. J. D., Bursik, M. I. & Atkinson, J. F. Settling-driven convection: A mechanism of sedimentation from stratified fluids. *J. Geophys. Res.* **104,** 7953–7966 (1999).
7. Wunsch, C. On oceanic boundary mixing. *Deep-Sea Res.* **17,** 293–301 (1970).
8. Buckingham, E. The principle of similitude. *Nature* **96,** 396–397 (1915).
9. Peacock, T., Stocker, R. & Aristoff, J. An experimental investigation of the angular dependence of diffusion-driven flow. *Phys. Fluids* **16,** 3503–3505 (2004).
10. Woods, A. W. Boundary-driven mixing. *J. Fluid Mech.* **226,** 625–654 (1991).
11. Page, M. A. & Johnson, E. R. Steady nonlinear diffusion-driven flow. *J. Fluid Mech.* **629,** 299–309 (2009).
12. Cordova-Figueroa, U. M. & Brady, J. F. Osmotic propulsion: The osmotic motor. *Phys. Rev. Lett.* **100,** 158303 (2008).
13. Prandtl, L. *The Essentials of Fluid Dynamics* (Blackie, 1952).
14. Oerlemans, J. & Grisogono, B. Glacier winds and parameterization of the related heat fluxes. *Tellus* **54A,** 440–452 (2002).
15. Ferrari, R. & Wunsch, C. Ocean circulation kinetic energy: Reservoirs, sources and sinks. *Annu. Rev. Fluid Mech.* **41,** 253–282 (2009).
16. Barad, M. F., Colella, P. & Schladow, S. G. An adaptive cut-cell method for environmental fluid mechanics. *Int. J. Numer. Meth. Fluids* **60,** 473–514 (2009).

Author contributions

T.P. conceived the original idea, supervised the research and wrote the manuscript. M.R.A. carried out the experiments, ran some numerical simulations and analysed the numerical data. M.F.B. ran the stratified flow simulations.